Nature of Manganese Species in $Ce_{1-x}Mn_xO_{2-\delta}$ Solid Solutions Synthesized by the Solution Combustion Route

B. Murugan and A. V. Ramaswamy*

Department of Chemistry, University of Pune, Pune-411 007, India

D. Srinivas, C. S. Gopinath, and V. Ramaswamy

Catalysis Division, National Chemical Laboratory, Pune-411 008, India

Received February 22, 2005. Revised Manuscript Received May 12, 2005

A series of manganese−cerium oxide composites with Mn concentrations in the range of 1−20 mol % in ceria was prepared by the solution combustion technique using urea as fuel. The nature, type, and oxidation state of Mn species in ceria were investigated by X-ray diffraction (XRD), diffuse reflectance UV−visible spectroscopy, electron paramagnetic resonance (EPR), X-ray photoelectron spectroscopy, and temperature-programmed reduction techniques. The study reveals that the method of preparation significantly influences the type of manganese species in ceria. Wet-impregnation, coprecipitation, and solid-state synthesis techniques lead to clustered MnO_x-like species in the ceria matrix, while the present method of preparation (solution combustion route) yields a highly dispersed form of Mn species. In the reported series of samples, Mn is present mainly in +2 and +3 oxidation states and there is no evidence for the presence of Mn^{4+} species. Powder X-ray diffraction studies at variable temperatures (298−1323 K) indicate the formation of $Ce_{1-x}Mn_xO_{2-\delta}$ solid solutions. No separate MnO_x-type phase was detected even at 1323 K. EPR studies reveal that the isolated Mn^{2+} and Mn^{3+} species are present in at least three different structural locations: species A, Mn ions in ceria−lattice defect sites; species B, Mn ions in framework Ce^{4+} locations; and species C, Mn ions in interstitial locations and at the surface of ceria. The Mn^{3+} ions in ceria exhibit a facile reduction and reoxidation behavior when exposed to dry hydrogen and subsequently to air at elevated temperatures. A highly dispersed state of Mn^{3+} and Mn^{2+} in ceria, facile redox behavior, and a synergistic Mn−ceria interaction are some of the unique properties of this material prepared by the solution combustion procedure.

1. Introduction

Cerium dioxide (CeO_2) is probably one of the most well-investigated oxides among the rare-earth metal oxides. It has attracted considerable interest as a catalyst, more as a promoter material in many catalyst formulations and as an electrode material in solid oxide fuel cells. The promoting influence of ceria in the alumina washcoats of three-way catalytic converters (TWC) and in the spray-dried, zeolite-based fluidized catalytic cracking formulations is well-known.[1−8] Interestingly, ceria may form a part of some very successful formulations of catalysts in many catalytic reactions in the future with environmental benefits.[9−11] In all these applications, there are two unique features associated with CeO_2 as a material of interest. One is the variable valence state of Ce, the $Ce^{4+} \leftrightarrow Ce^{3+}$ redox couple (1.3−1.8 V) being amenable for a shift between CeO_2 and Ce_2O_3 under oxidizing and reducing conditions, respectively. At low oxygen partial pressures and elevated temperatures, ceria easily releases oxygen to form $CeO_{2-\delta}$ and the oxygen deficiency is charge-compensated by the formation of Ce^{3+}.[12] This gives rise to a second feature, which is the ease of formation of labile oxygen vacancies and, associated with it, the relatively high mobility of bulk oxygen species. Ceria, thus, acts as an oxygen buffer, by storing and releasing oxygen under controlled conditions, a unique property that is taken advantage of in the TWC formulations for the fluctuating fuel-rich and lean-burn conditions of gasoline engines.

Ceria crystallizes in the cubic fluorite structure, with cations in eightfold and anions in fourfold coordination. By

* To whom correspondence should be addressed. E-mail: avram@chem.unipune.ernet.in.

(1) Martín, L.; Arranz, J. L.; Prieto, O.; Trujillano, R.; Holgado, M. J.; Galán, M. A.; Rives, V. *Appl. Catal. B* **2003**, *44*, 41.
(2) Lox, E. S. J.; Engler, B. H. In *Environmental Catalysis*; Ertl, G., Knözinger, H., Weitkamp. J., (Eds.; Wiley: New York, 1999; p. 1.
(3) Trovarelli, A., Ed. *Catalysis by Ceria and Related Materials*; Imperial College Press: London, 2002.
(4) Iglesias-Juez, A.; Martínez-Arias, A.; Hungría, A. B.; Anderson, J. A.; Conesa, J. C.; Soria, J.; Fernández-García, M. *Appl. Catal. A* **2004**, *259*, 207.
(5) Gandhi, H. S.; Graham, G. W.; McCabe, R. W. *J. Catal.* **2003**, *216*, 433.
(6) Shi, Z. M.; Liu, Y.; Yang, W. Y.; Liang, K. M.; Pan, F.; Gu, S. R. *J. Eur. Ceram. Soc.* **2002**, *22*, 1251.
(7) Trovarelli, A. *Catal. Rev.−Sci. Eng.* **1996**, *38*, 439.
(8) Trovarelli, A.; de Leitenburg, C.; Boaro, M.; Dolcetti, G. *Catal. Today* **1999**, *50*, 353.
(9) Matatov-Meytal, Y. I.; Sheintuch, M. *Ind. Eng. Chem. Res.* **1998**, *37*, 309.
(10) Liu, W.; Flytzani-Stephanopoulos, M. *J. Catal.* **1995**, *53*, 317.
(11) Sahibzada, M.; Steele, B. C. H.; Zheng, K.; Rudkin, R. A.; Metcalfe, I. S. *Catal. Today* **1997**, *38*, 459.
(12) Kim, S.; Merkle, R.; Maier, J. *Surf. Sci.* **2004**, *549*, 196 and references therein.

10.1021/cm050401j CCC: $30.25
Published on Web 06/21/2005

itself, ceria has limited application as a catalytic material, rather a poor support compared to alumina, silica−alumina, and others, both from the chemical nature of the material as well as from its textural properties. It has poor thermal stability and gets deactivated due to sintering at high temperatures, thereby losing its oxygen storage capacity. However, the unique properties of ceria are retained and are even enhanced by the formation of mixed oxides of ceria with many cations, such as Zr^{4+}, Si^{4+}, Al^{3+}, La^{3+}, and others.[13,14] In this context, transition metal oxides such as MnO_2, Mn_2O_3, CuO, Cr_2O_3, and V_2O_5, which themselves are active in many redox reactions, have been incorporated in the matrix of ceria as composites with additional advantages, and these have great potential as catalysts for low-temperature oxidation of CO and selective catalytic reduction (SCR) of NO_x.[15−22]

With the possibility of multiple valencies for Mn and the redox couple associated with Ce, the mixed MnO_x−CeO_2 samples are interesting materials for further detailed investigations both from the structural and from the spectral understanding of the system as well as for further application of them in other oxidation−reduction reactions. It is also very pertinent to note here that the method of preparation of almost all the mixed oxides is beset with uncertainties in the resulting interaction between the two oxides, particularly when one of them is a minor component and is the active phase for a particular catalytic reaction. The method of preparation significantly influences the properties of the resulting materials, due to differences in the long-range order as well as molecular interactions, which in turn influence their application as sensors, catalysts, or electronic materials. While comparing the MnO_x−CeO_2 samples prepared by three different methods, namely, coprecipitation, impregnation, and citric acid methods, Qi and Yang[17] found that the sample having a definite concentration of MnO_x in CeO_2, prepared by the citric acid method and calcined at 923 K, was highly active in SCR of NO_x. The high activity has been attributed to the highly dispersed Mn species and more active oxygen species that are formed. This is positively due to the different types of Mn species present in/on the ceria matrix. The recent reports by Bera et al., on the other hand, highlight a novel route for metal ion dispersion, namely, "solution combustion synthesis".[23−28] This route produced materials with a high order of metal ion dispersions and paved the way for the formation of solid solutions. The application of the solid solution on various catalytic reactions has been illustrated in these reports.[23−28] An understanding of the structural and spectral aspects of the system based on the method of preparation is of great importance for improving the efficiency of these materials in many applications.

In the present study the solution combustion route was chosen to incorporate Mn in the ceria lattice. The Mn/CeO_2 samples, with different Mn contents in the ceria matrix, have been prepared and characterized by normal and high-temperature X-ray diffraction (HTXRD) followed by Rietveld refinement of the profiles to get structural information. Electron paramagnetic resonance (EPR) spectroscopy is used effectively to study the environment and reversible redox property of Mn/CeO_2 samples due to its high sensitivity. The synergistic effect of Ce^{4+} and Mn^{n+} that alters the redox properties of the metal ion is well-illustrated by temperature-programmed reduction (TPR) and EPR techniques. We highlight in this report some of the unique properties of this material, while comparing Mn−ceria samples of similar compositions prepared by coprecipitation and wet-impregnation techniques.

2. Experimental Section

2.1. Synthesis. A series of $Ce_{1-x}Mn_xO_{2-\delta}$ solid solutions, where $x = 0.01$, 0.02, 0.03, 0.04, 0.05, 0.1, and 0.2 was prepared by the solution combustion synthesis method[25] using urea as fuel. In a typical synthesis for the preparation of 1 mol % Mn/CeO_2, cerous nitrate (6 g), manganese acetate (0.0342 g), and urea (3.98 g) were dissolved in distilled water (10 mL) taken in a 500-mL beaker. This was then introduced into a muffle furnace maintained at 723 K. The solution got ignited and burnt with a flame yielding a voluminous solid material within 5 min. The solid product was recovered immediately after the completion of the combustion process. The other compositions of Mn/CeO_2 solid solutions were prepared in a similar manner. Pure ceria and pure MnO_x samples were also prepared by the same method.

For comparison, two samples of Mn/CeO_2 (5 and 20 mol % Mn in ceria) have been prepared by the incipient wetness impregnation procedure. Pure ceria prepared as above was impregnated with an aqueous solution of Mn−acetate of appropriate concentrations, dried at 383 K, and then calcined at 723 K in air for 6 h. Two more samples of similar compositions have been prepared by the low-temperature coprecipitation technique. Briefly, an aqueous solution containing stoichiometric amounts of Mn−acetate and cerous nitrate was added to a calculated amount of concentrated NH_4OH solution under continuous stirring. The final pH of the resulting mixture was adjusted to 9. The hydroxide precipitate was filtered, washed, dried at 383 K overnight, and then calcined at 723 K for 6 h in air.

2.2. Characterization. The normal powder X-ray diffraction (PXRD) data of the sample for Rietveld refinement was collected on a Rigaku X-ray diffractometer (model DMAX IIIVC) equipped with a Ni filtered Cu Kα ($\lambda = 1.542$ Å, 40 kV, 20 mA) radiation and graphite crystal monochromator. The data were collected in

(13) Garcia, M. F.; Arias, A. M.; Hanson, J. C.; Rodriguez, J. A. *Chem. Rev.* **2004,** *104*, 4063 and references therein.
(14) Miki, T.; Ogawa, T.; Haneda, M.; Kakuta, N.; Ueno, A.; Tateishi, S.; Matsuura, S.; Sato, M. *J. Phys. Chem.* **1990**, *94*, 6464. Reddy, B. M.; Khan, A.; Yamada, Y.; Kobayashi, T.; Loridant, S.; Volta, J. C. *J. Phys. Chem. B* **2002**, *106*, 10964.
(15) Shan, W.; Shen, W.; Li, C. *Chem. Mater*. **2003**, *15*, 4761.
(16) Bera, P.; Priolkar, K. R.; Sarode, P. R.; Hegde, M. S.; Emura, S.; Kumashiro, R.; Lalla, N. P. *Chem. Mater*. **2002**, *14*, 3591.
(17) Qi, G.; Yang, R. T. *J. Catal.* **2003**, *217*, 434.
(18) Qi, G.; Yang, R. T. *J. Phys. Chem. B* **2004**, *108*, 15738.
(19) Long, R. Q.; Yang, R. T.; Chang, R. *Chem. Commun*. **2002**, *5*, 452.
(20) Harrison, P. G.; Daniell, W. *Chem. Mater*. **2001**, *13*, 1708.
(21) Matta, J.; Courcot, D.; Abi-Aad, E.; Aboukais, A. *Chem. Mater*. **2002**, *14*, 4118.
(22) Machida, M.; Uto, M.; Kurogi, D.; Kijima, T. *Chem. Mater*. **2000**, *12*, 3158
(23) Bera, P.; Aruna, S. T.; Patil, K. C.; Hegde, M. S. *J. Catal*. **1999**, *186*, 36.
(24) Bera, P.; Priolkar, K. R.; Gayen, A.; Sarode, P. R.; Hegde, M. S.; Emura, S.; Kumashiro, R.; Jayaram, V.; Subbanna, G. N. *Chem. Mater*. **2003**, *15*, 2049.
(25) Bera, P.; Patil, K. C.; Jayaram, V.; Hegde, M. S.; Subbanna, G. N. *J. Mater. Chem*. **1999**, *9*, 1801.
(26) Bera, P.; Patil, K. C.; Jayaram, V.; Hegde, M. S.; Subbanna, G. N. *J. Catal*. **2000**, *196*, 293.
(27) Bera, P.; Hegde, M. S. *Catal. Lett*. **2002**, *79*, 75.
(28) Bera, P.; Patil, K. C.; Hegde, M. S. *Phys. Chem. Chem. Phys*. **2000**, *2*, 373.

the 2θ range of 20−110° with a step size of 0.02° and a scan rate of 0.5° min^{-1}. The sample was rotated throughout the scan for better counting statistics. The observed interplanar *d* spacing was corrected with respect to silicon. Rietveld refinement of the PXRD profiles was carried out using the X′ Pert Plus software.

The high-temperature experiments (HTXRD) were carried out in static air using an Anton Paar high-temperature attachment (HTK-16) to a Philips X′ Pert Pro diffractometer, equipped with an Fe filtered Co Kα (λ = 1.790 31 Å, 40 kV, 30 mA) radiation. The sample was mounted on a platinum strip, which acted as the sample holder as well as the heating element. To the bottom of the platinum strip was soldered a Pt/Pt−Rh thermocouple. The data were collected in the 2θ range of 20−110° with a step size of 0.02° and scan rate of 1° min^{-1} at different temperature intervals in the range of 298−1323 K. The sample was heated at a rate of 5 K min^{-1}, and a soak time of 10 min was employed at each temperature before the scan.

Diffuse reflectance UV−visible (DRUV−vis) spectra were recorded on a JASCO V-570 spectrophotometer in the diffuse reflectance mode. The reduction and reoxidation of the samples were carried out at 773 K in a flow of dry hydrogen (20 mL min^{-1}) and at 573 K in the flow of dry air (20 mL min^{-1}), respectively.

TPR experiments were performed using a Micromeritics Autochem 2910 instrument. A weighed amount of the sample (≈125 mg) was placed in a quartz reactor, pretreated in a flow of Ar (99%) gas at 773 K for 1 h (ramp rate of 10 K min^{-1}), and cooled to room temperature. A gas mixture of H_2 (5%)−Ar (95%) was then passed (25 mL min^{-1}) through the reactor. The temperature was raised to 973 K at a heating rate of 10 K min^{-1}. A thermal conductivity detector was employed at the outlet of the reactor to measure the volume of hydrogen consumed during reduction of the samples.

EPR measurements were conducted on a Bruker EMX X-band spectrometer ($\upsilon \approx 9.4$ GHz) operating at 100-kHz field modulation. The as-synthesized sample (≈80 mg) was taken in a specially designed quartz EPR cell (o.d. = 4 mm) fitted with greaseless stopcocks with provision for adsorption and desorption of gases. Prior to EPR measurements, the samples were degassed at various temperatures for 2 h (0.1333 Pa) and then treated with dry hydrogen (20 mL min^{-1}) for 2.5 h at different temperatures. The reoxidation of the samples was carried out at 573 K unless otherwise mentioned. The spectra were recorded at 298 K for all the samples.

The photoemission spectra were recorded on a VG Microtech Multilab ESCA 3000 spectrometer using a nonmonochromatized Mg Kα X-ray source ($h\upsilon$ = 1253.6 eV). Base pressure in the analysis chamber was maintained in the $4-8 \times 10^{-8}$ Pa range. The energy resolution of the spectrometer was set at 0.8 eV with Mg Kα radiation at a pass energy of 20 eV. Binding energy (BE) calibration was performed with the Au($4f_{7/2}$) core level at 83.9 eV. The BE of adventitious carbon (284.9 eV) was utilized for charge correction. The error in all the BE values reported here is within 0.1 eV.

3. Results and Discussion

3.1. PXRD. PXRD data were collected for "pure" CeO_2 and Mn/CeO_2 samples in the 2θ range of 20−110° with a step size of 0.02° and a scan rate of 0.5°/min. Rietveld refinement analysis (see Figure 1, for example, for 5 mol % Mn/CeO_2) indicated that the XRD pattern could be indexed satisfactorily to the fluorite structure with a space group *Fm*3*m*. The values of the lattice parameters and oxygen ion vacancies for all the samples are listed in Table 1. Oxygen ion vacancies increased with Mn content (Figure 2) indicating

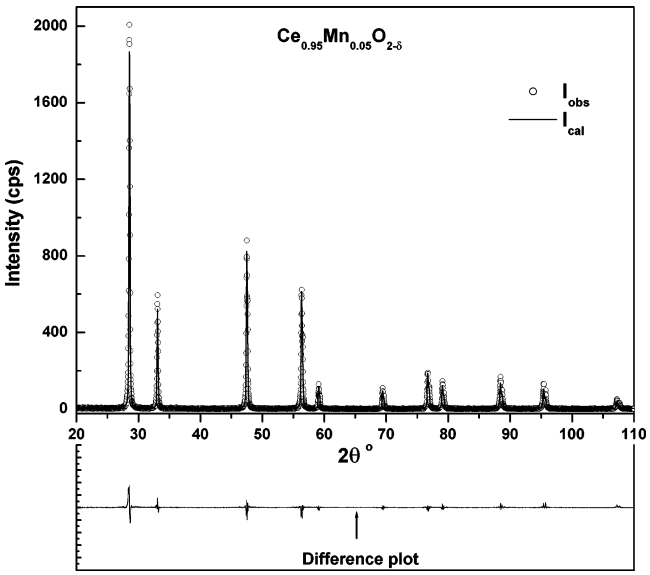

Figure 1. Rietveld refinement profile of the 5 mol % Mn/CeO_2 sample prepared by the combustion route. I_{obs} and I_{cal} are the observed and calculated intensities, respectively. The difference plot is given at the bottom.

Table 1. Crystallographic Data of the Pure Ceria and Mn/Ceria Samples[a]

	lattice parameter		
[Mn]/[Mn + Ce]	*a* (Å)	volume (Å^3)	oxygen vacancy (δ)
0	5.4124	158.55	0.11
0.01	5.4120	158.51	0.14
0.02	5.4118	158.50	0.16
0.03	5.4111	158.44	0.17
0.04	5.4110	158.43	0.21
0.05	5.4101	158.35	0.29
0.20	5.4059 (5.4120)	157.98 (158.52)	0.43 (0.13)

[a] The values in the parentheses correspond to the wet-impregnated sample.

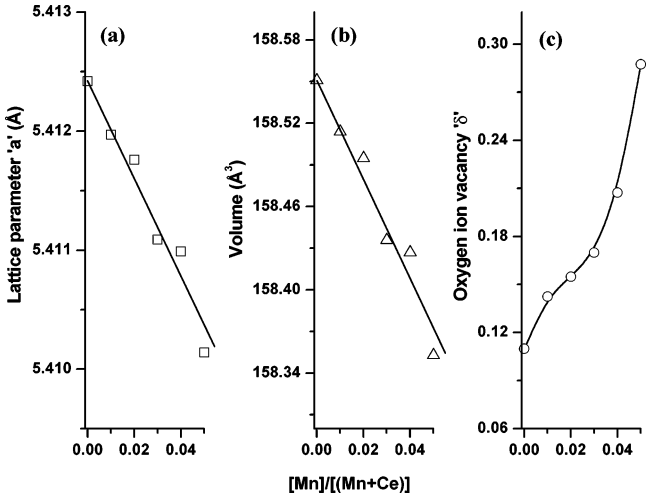

Figure 2. Dependence of the (a) lattice parameter, (b) volume, and (c) oxygen ion vacancy with [Mn]/[Mn + Ce].

that Mn ions are possibly substituted for Ce^{4+} in the fluorite lattice. Although the absolute value of the oxygen ion vacancy is not very reliable, a systematic increase in the vacancy with Mn concentration can certainly be discernible from the Rietveld refinement analysis. A similar observation was also noted by Bera et al.[16] for their Cu/CeO_2 samples. If there is any incorporation of Mn ions in the Ce^{4+} site, the

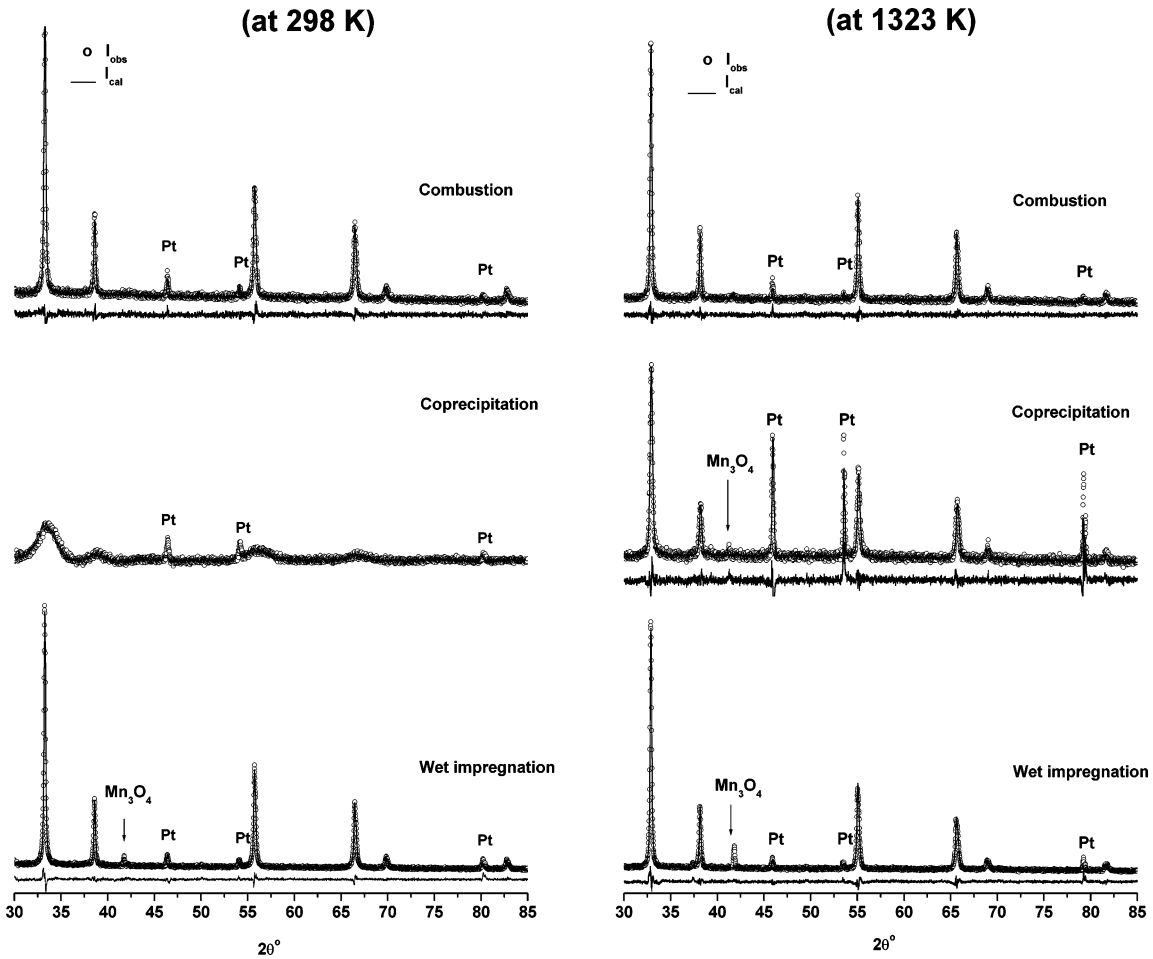

Figure 3. Rietveld refinement XRD profiles of 20 mol % Mn/CeO_2 samples prepared by different methods and scanned at 298 and 1323 K. I_{obs} and I_{cal} are the observed and calculated intensities, respectively. The difference plot is given at the bottom of each XRD profile. The refinement could not be done for the coprecipitated sample due to the broad nature of the peaks. Peaks arising from the Mn_3O_4 phase and platinum sample holder are indicated.

lattice parameter should decrease, because the ionic radius of Mn^{n+} (Mn^{2+} = 0.83 Å, Mn^{3+} = 0.645 Å, and Mn^{4+} = 0.53 Å) is smaller than that of Ce^{4+} (1.01 Å). Indeed, a decrease in the lattice parameter from 5.4124 Å (for "pure" ceria) to 5.4101 Å (for 5 mol % Mn/CeO_2) is observed, confirming that some Mn^{n+} ions are incorporated in the ceria lattice forming homogeneous $Ce_{1-x}Mn_xO_{2-\delta}$ solid solutions ($x = 0.01-0.05$). There is hardly any change in the lattice parameter of the Mn sample (20 mol % Mn/CeO_2) prepared by wet-impregnation of ceria. This indicates that there is no Mn substitution in the cubic lattice of ceria.

The PXRD pattern (peak widths) indicated that the samples are highly crystalline. The crystallite size of ceria is little influenced by Mn doping. The size increased marginally from 41 nm for "pure" ceria to 51 nm for Mn-containing CeO_2. A further increase in the concentration of Mn did not affect the crystallite size. This suggests that Mn ions initially get incorporated into the defect sites, which are the possible causes for the sintering of ceria. Above this critical concentration, Mn occupies the lattice sites possibly at outer layers of the crystallites. Further evidence for this comes from X-ray photoelectron spectroscopy (XPS) results discussed later on in this report. The presence of a separate MnO_x-like phase was not detected even when the Mn/CeO_2 samples were thermally treated at 1323 K (Figure 3). This observation indicates that the Mn species are present in a highly dispersed state. Pure manganese oxide prepared by the same urea combustion method is composed of Mn_3O_4 and MnO phases with Mn ions in +2 and +3 oxidation states (Figure 4). No MnO_2-like phase (Mn oxidation state + 4) was detected.

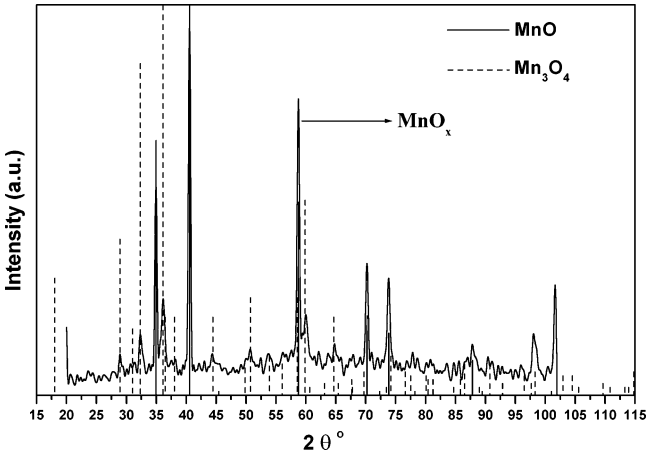

Figure 4. XRD of MnO_x prepared by the solution-combustion route. The dashed and solid lines mark standard Mn_3O_4 and MnO peaks, respectively.

At this juncture, it may be noted that the method of preparation influences the nature of Mn species formed. We find considerable differences in the structural features of the samples prepared by coprecipitation and wet-impregnation procedures. A comparison of the Rietveld refined XRD

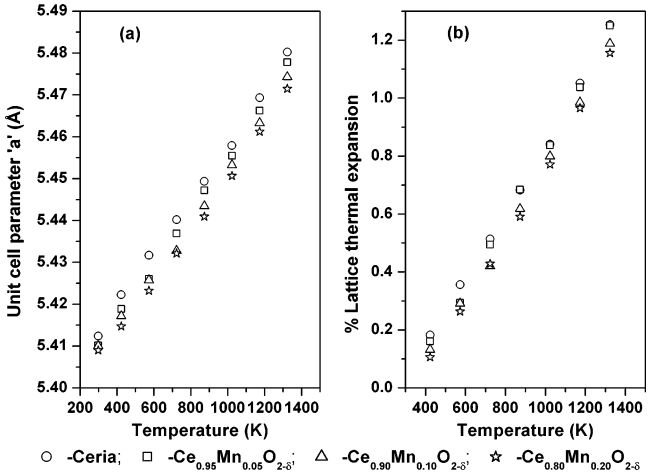

Figure 5. (a) Variation of the unit cell parameter "*a*" and (b) percent lattice thermal expansion of the Mn/CeO_2 samples prepared by the combustion method as a function of temperature.

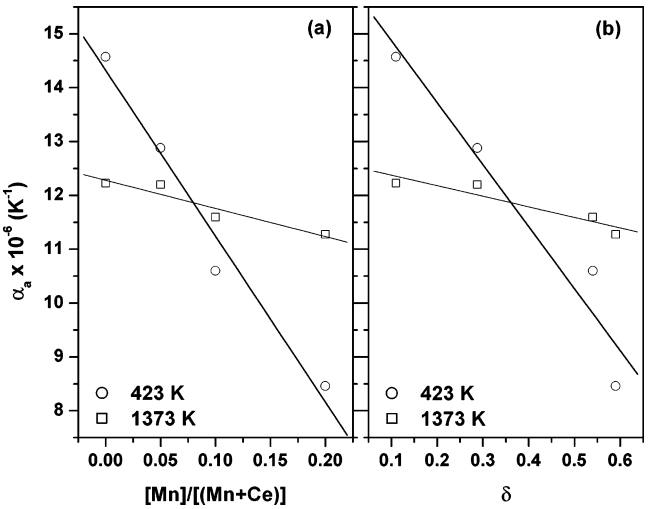

Figure 6. Lattice thermal expansion coefficient of Mn/CeO_2 samples prepared by the combustion route as a function of (a) Mn concentration and (b) oxygen vacancy (δ).

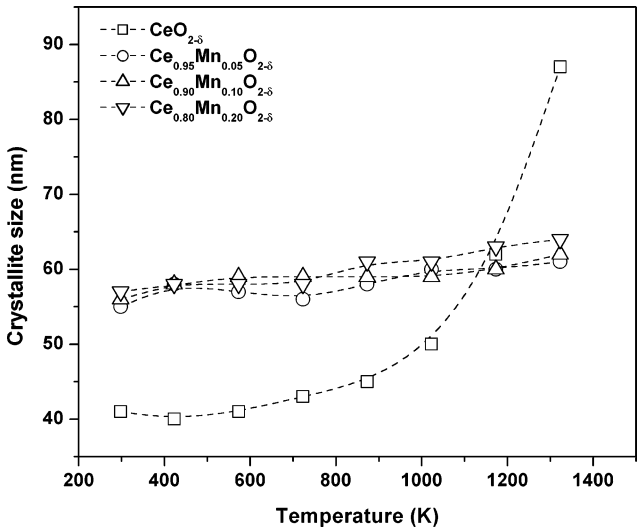

Figure 7. Dependence of crystallite size with temperature of CeO_2 and Mn/CeO_2 samples prepared by the combustion route.

profiles of three Mn/CeO_2 samples (20 mol % Mn) prepared by different procedures is given in Figure 3. The coprecipitated Mn/CeO_2 sample is poorly crystalline, showing broad XRD peaks due to very small particles. The sample prepared by the wet-impregnation procedure showed narrower features, and the XRD pattern could be satisfactorily refined to the fluorite structure (space group *Fm*3*m*). A distinct Mn_3O_4 phase is detected in samples prepared by the wet-impregnation and coprecipitation routes. Such a phase is absent in all Mn/CeO_2 samples prepared by the combustion method, up to a 20 mol % Mn concentration (Figure 3). The present method of synthesis, using urea as fuel, confines Mn to +2 and +3 oxidation states in Mn/CeO_2 samples. Spectroscopic analysis of the samples, described in the subsequent sections, indeed provides unequivocal evidence to this conclusion.

3.2. HTXRD. The thermal stability and thermal expansion of Mn/CeO_2 solid solutions (combustion route) were investigated by in situ HTXRD analysis, in the temperature range of 298−1323 K. An analysis of the in situ HTXRD data for the samples prepared by the solution combustion method indicates that the unit cells of CeO_2 and Mn/CeO_2 expand linearly with temperature (Figure 5a,b). The thermal expansion coefficient (α_a) decreases linearly with an increase in the Mn concentration and oxygen ion vacancy (δ; Figure 6a,b). This variation in α_a with Mn concentration is due to partial Mn substitution in the ceria lattice. The Mn−O bond is covalent while the Ce−O bond is ionic in nature due to Ce being more electropositive. It is known that ionic solids have higher α_a compared to covalent solids.[29] Thus, Mn incorporation in the ceria lattice affects α_a. A large decrease in α_a with an increase in Mn loading reconfirms substitution of Ce by Mn ions.

In situ HTXRD studies reveal that the crystallite size of pure CeO_2 increases continuously (from 41 to 94 nm) with an increase in the temperature from 298 to 1323 K. Such a variation in crystallite size is only marginal in Mn containing CeO_2 samples (see Figure 7). The structural integrity at high temperatures of the samples prepared by coprecipitation and wet-impregnation was investigated by subjecting these samples (20 mol % Mn in ceria) to in situ HTXRD studies. A comparison of the Rietveld refined XRD profiles of the samples is presented in Figure 3. The samples prepared by the coprecipitation procedure become highly crystalline due to sintering of smaller particles, and Mn_3O_4 phases become apparent in samples prepared by wet-impregnation and coprecipitation procedures. It is interesting to note that incorporation of Mn in ceria through the solution combustion technique prevents ceria from sintering at high temperatures (Figure 7), while there is a continuous sintering of ceria through the temperature range in the coprecipitated Mn/CeO_2 sample of similar composition.

3.3. DRUV−Vis Spectroscopy. Pure CeO_2 and Mn-containing CeO_2 samples prepared by the combustion method show partially resolved $O^{2-} \rightarrow Ce^{4+}$ charge transfer bands at 266 and 345 nm. The former is a specular reflectance band arising from the surface sites while the latter is a diffuse reflectance band originating from the bulk CeO_2. A representative spectrum for 1 mol % Mn/CeO_2 is shown in Figure 8a. The Mn-containing samples showed additionally a broad

(29) Ramaswamy, V.; Awati, P.; Tyagi, A. K. *J. Alloys Compd.* **2004**, *364*, 180.

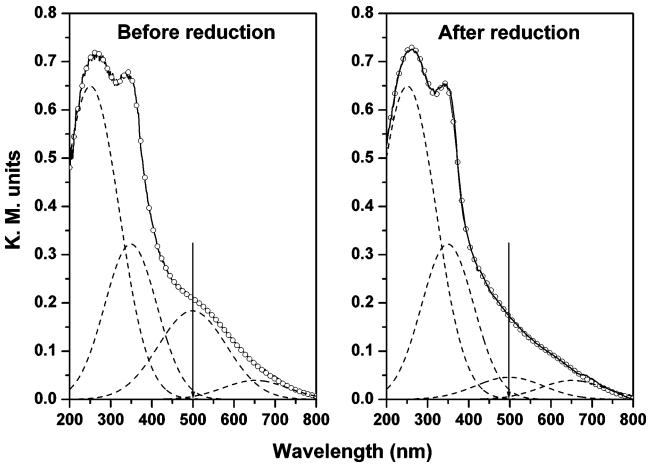

Figure 8. DRUV−vis spectrum of the $Ce_{0.99}Mn_{0.01}O_{2-\delta}$ sample prepared by the combustion route. (a) Before reduction and (b) after reduction with dry hydrogen at 773 K. All the other Mn-containing samples prepared by the combustion route showed similar type spectra.

feature in the visible region. Such a feature was observed also in the case of Mn−MCM-41.[30,31] It was attributed to the presence of Mn^{3+} species.[30,31] The experimental spectrum of the ceria samples was fitted with the Gaussian curves to identify the component bands. The broad visible feature could be deconvoluted into two bands with maxima at 497 and 647 nm, respectively. The former band could be attributed to the $^5E_2 \rightarrow {}^5T_2$ transition of Mn^{3+} species[32−34] as well as to the $^6A_1 \rightarrow {}^4T_2$ transition of Mn^{2+} species.[35] Mn^{3+} in "pure" Mn_2O_3 shows this band at a higher energy (475 nm). Dispersion of Mn^{3+} ions and Mn−ceria interactions are the probable causes for the shift of the visible band toward lower energy. Mn^{2+} ions in "neat" MnO showed a band 610 nm which is due to the $^6A_1 \rightarrow {}^4T_1$ transition.[35] This band in the Mn/CeO_2 samples occurs at longer wavelengths (647 nm) again due to strong −Mn−O−Ce− interactions. The Mn concentration does not affect the band position, indicating that the Mn ions are highly dispersed through the concentration range studied.

Significant changes were observed in the UV−visible spectrum when the Mn/CeO_2 samples were reacted with dry hydrogen at elevated temperatures (e.g., 773 K). A typical spectrum of hydrogen-treated 1 mol % Mn/CeO_2 is shown in Figure 8b. On reduction with hydrogen, the band at 495 nm, which was attributed to Mn^{3+}/Mn^{2+} ions in the ceria matrix, decreased in intensity (compare the curve in Figure 8b with the curve in Figure 8a) suggesting that Mn^{3+} ions get reduced to Mn^{2+} ions. It may be noted that the band for Mn^{2+} ions has a low extinction coefficient, because it is spin-forbidden. The band reappeared on treating the reduced sample with air at 573 K, suggesting that the Mn^{3+} to Mn^{2+} conversion is reversible. EPR spectroscopy provides additional evidence for the facile reduction/oxidation of Mn ions upon treatment with dry hydrogen/air at elevated temperatures.

DRUV−vis spectra of Mn/CeO_2 samples prepared by coprecipitation and wet-impregnation procedures reveal some interesting differences from those of the earlier samples with respect to the type of Mn species and their interaction with ceria. A comparison of the UV−visible spectral features of Mn/CeO_2 samples of similar compositions (5 mol % Mn in ceria) prepared by the three methods is given in Table 2. On the basis of a rough estimate of the intensities of the bands in the region, 465−495 (for Mn^{3+}) and 605−647 nm (for Mn^{2+}) for the three samples, we may note that the ratio of Mn^{3+} to Mn^{2+} ions in the samples is in the order, combustion synthesis > coprecipitation > wet-impregnation methods of preparation of the samples. Apart from the differences in Mn^{3+} and Mn^{2+} concentrations, a marked shift in the band position is also observed. The shift of the bands to the lower energy side suggests that dispersion of Mn species and −Mn−O−Ce− interactions increase in samples of different preparations in the order, wet-impregnation < coprecipitation < solution combustion methods.

3.4. TPR. Figure 9a presents the TPR profiles of Mn/CeO_2 and MnO_x samples prepared by the combustion procedure as a function of reduction temperature. Pure ceria shows two reduction maxima at about 820 and 1100 K (not shown in the figure) associated with surface and bulk reduction, respectively.[36,37] The amount of hydrogen consumption, T_{max}, and T_{onset} of reduction of different samples are summarized in Table 3. The peak reduction temperature of MnO_x prepared by the combustion method is about 737 K. The reduction onset temperature of the MnO_x is around 620 K. The T_{max} at 737 K for MnO_x suggests that the reducible Mn could be of type Mn_3O_4.[38,39] However, the amount of hydrogen uptake is calculated to be 43 mL g^{-1}, which is less than that required to reduce the Mn^{3+} ion in pure Mn_3O_4. This suggests that the MnO_x formed by this method might be a mixture of Mn_3O_4 and MnO. The XRD analysis of the samples has earlier arrived at a similar conclusion (see Figure 4). The onset temperature of reduction (T_{onset}) of Mn/ceria was less than that of MnO_x. This can be attributed to the presence of Ce, which can modify the redox activity of Mn. The 1 mol % Mn/CeO_2 sample shows a broad reduction profile starting from 414 K with a peak at 605 K. This broad profile indicates a poor reduction process. This may be due to most of the Mn ions being dissolved into the ceria matrix in a difficult-to-reduce environment and a very small amount being present in the reducible form (i.e., Mn^{3+} state). The 3 mol % Mn/CeO_2 sample shows a peak maximum at 613 K. A significant decrease in the reduction temperature of Mn^{3+} ions in CeO_2 at 613 K and below compared to 737 K in pure MnO_x clearly demonstrates the absence of any large individual crystallites or islands of the MnO_x phase in this sample. The T_{max} increases with an increase in Mn concentration, and this may be due to the

(30) Aronson, B. J.; Blanford, C. F.; Stein, A. *J. Phys. Chem. B* **2000**, *104*, 449.
(31) Maruyama, T.; Osaki, Y. *J. Electrochem. Soc.* **1995**, *142*, 3137.
(32) McClure, D. S. *J. Chem. Phys.* **1962**, *36*, 2757.
(33) Kijlstra, W. S.; Poels, E. K.; Bliek, A.; Weckhuysen, B.; Schoonheydt, R. A. *J. Phys. Chem. B* **1997**, *101*, 309.
(34) Shen, X. M.; Clearfield, A. *J. Solid State Chem.* **1986**, *64*, 270.
(35) Pratt, G. W.; Coelho, R. *Phys. Rev.* **1959**, *116*, 281.
(36) Terribile, D.; Trovarelli, A.; de Leitenburg, C.; Primavera, A.; Dolcetti, G. *Catal. Today* **1999**, *47*, 133.
(37) Yao, H. C.; Yao, Y. F. Y. *J. Catal.* **1984**, *86*, 254.
(38) Wolfovich, M. A.; Landau, M. V.; Brenner, A.; Herskowitz, M. *Ind. Eng. Chem. Res.* **2004**, *43*, 5089.
(39) Hussain, S. T.; Sayari, A.; Larachi, F. *Appl. Catal. B* **2001**, *34*, 1.

Table 2. DRUV−Vis Spectral Features of the 5 mol % Mn/CeO_2 Sample Prepared by Different Routes

method of preparation	specular reflectance band (nm)	diffuse reflectance band (nm)	$^5E_2 \rightarrow {}^5T_2$ transition (nm)	$^6A_1 \rightarrow {}^4T_2$ transition (nm)	Mn^{3+}/Mn^{2+} ratio[a]
combustion	264	343	495	647	6.9
coprecipitation	246	330	491	610	2.5
wet-impregnation	254	341	468	605	1.8

[a] The Mn^{3+}-to-Mn^{2+} ratio was calculated from the integrated area under the bands.

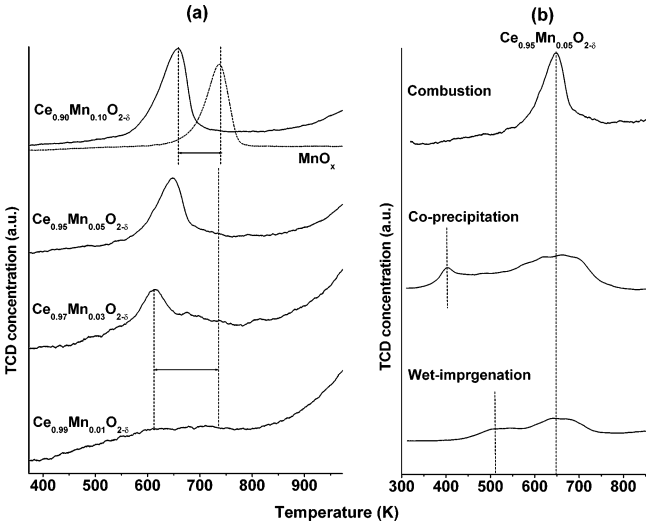

Figure 9. (a) TPR profile of Mn−ceria and MnO_x samples prepared by the combustion method. (b) TPR profile of the 5 mol % Mn/CeO_2 sample prepared by different synthesis procedures.

Table 3. Reduction Properties of $Ce_{1-x}Mn_xO_{2-\delta}$ Solid Solutions

sample	H_2 consumed (mL/g)	T_{onset} (K)	T_{max} (K)	reducible oxide (%)
$Ce_{0.99}Mn_{0.01}O_{2-\delta}$		414	605	n.d.
$Ce_{0.97}Mn_{0.03}O_{2-\delta}$	0.50	450	613	26
$Ce_{0.95}Mn_{0.05}O_{2-\delta}$	2.20	506	648	67
$Ce_{0.95}Mn_{0.05}O_{2-\delta}$[a]	0.38	403	511, 647	12
$Ce_{0.95}Mn_{0.05}O_{2-\delta}$[b]	0.53	327	408, 511, 647	16
$Ce_{0.90}Mn_{0.10}O_{2-\delta}$	4.30	520	659	65
MnO_x	43.0	620	737	66

[a] Wet-impregnated sample. [b] Coprecipitated sample.

formation of dispersed Mn oxides at higher loadings. Even if the Mn loading was increased to 10 mol %, only a partial amount of Mn gets dissolved into the ceria matrix. The excess amount of Mn resides as dispersed oxide on the surface of the ceria. The reducible Mn species in this oxide island do not have a strong interaction with ceria as in the case of samples with low concentrations of Mn in ceria. Hence, there is an increase in the T_{max} value with an increase in Mn concentration. The TPR study also indicates that Mn^{3+} ions in Mn/CeO_2 samples can be reduced at a lower temperature than that of the Mn^{3+} ion in MnO_x. This could be possible when Mn^{3+} ions are in the near neighborhood of Ce^{4+} ions and there exists some interaction between Mn^{3+} and Ce^{4+} ions. A synergistic effect between Mn^{3+} and Ce^{4+} ion pairs might promote Mn^{3+} reduction at a lower temperature than in the MnO_x. Even though a good correlation from the hydrogen consumption could not be derived for Ce^{4+} reduction, in situ EPR investigations evidenced the signals for the Ce^{3+} ion in the temperature range of Mn reduction in Mn/ceria samples.

A comparison of TPR profiles of Mn/CeO_2 (5 mol %) samples prepared by the combustion, wet-impregnation, and coprecipitation techniques is given in Figure 9b. From the fingerprint reduction profiles of each sample, we find considerable differences in the nature and reducibility of Mn species in ceria. The sample prepared by the wet-impregnation method is not constituted by a single MnO_x phase but apparently possesses a mixture of oxides. The reduction profile is broad extending from 375 to 750 K. The shape of the reduction profile and the observed T_{max} suggest the presence of both Mn_3O_4 and Mn_2O_3 in ceria.[53] Further, the reduction process suggests that one or more adlayers of Mn_2O_3 have been formed, which allows a two-step reduction via Mn_3O_4.[54] On the other hand, the Mn/CeO_2 sample prepared by the coprecipitation procedure shows a sharp reduction peak with T_{max} at 408 K, which could be ascribed to the reduction of Mn^{4+} species. In addition, we also notice the presence of Mn_3O_4 and Mn_2O_3 species. The amount of hydrogen consumption for the 5 mol % Mn/CeO_2 samples prepared by the three methods falls in the order solution combustion > coprecipitation > wet-impregnation (Table 3). Hence, more reducible MnO_x (as Mn^{3+} species) is present in the case of samples prepared by the combustion method. These results are further supported by DRUV−vis and EPR spectroscopic observations.

3.5. XPS. The XPS spectra of the core levels of Mn(2p) and Mn(3s) in 1, 5, and 10 mol % Mn/CeO_2 (combustion route) are shown in Figure 10. The $Mn(2p_{3/2})$ core level at 641.3 eV can be attributed to Mn in +2 as well as in +3 oxidation states. Because the BEs of Mn^{2+} and Mn^{3+} are very close to each other,[40] a distinct identification of the oxidation state is not possible. The BE of Mn^{4+} (642.4 eV) is, however, significantly different[40] from those of the Mn^{2+} (641.0 eV) and Mn^{3+} (641.4 eV) ions. Nonetheless, the Mn(3s) peak splitting widths for different Mn oxides (Table 4) are helpful to find out the oxidation state.[41−43] The oxidation states of the sample are identified through direct comparison to standard values from literature. Accordingly, a Mn(3s) splitting width ΔE of 5.6 eV (for 1, 5, and 10 mol % Mn/CeO_2) corresponds to a mixed valence of +2 and +3. The XPS results of Mn/CeO_2 do not provide any evidence for the presence of Mn^{4+} species. It may be recalled that MnO_x too, prepared by the present method using urea as fuel, did

(40) *Handbook of X-ray Photoelectron Spectroscopy*; Wagner, C. D., Riggs, W. M., Davis, L. E., Moulder, J. F., Mullerberg, G. E., Eds.; Perkin-Elmer Corp.: Eden Prairie, MN, 1979.
(41) Djurfors, B.; Broughton, J. N.; Brett, M. J.; Ivey, D. G. *Acta Mater.* **2005**, *53*, 957.
(42) Chigane, M.; Ishikawa, M. *J. Electrochem. Soc.* **2000**, *147*, 2246. Carver, J. C.; Schweitzer, G. K.; Carlson, T. A. *J. Chem. Phys.* **1972**, *57*, 973.
(43) Toupin, M.; Brousse, T.; Bélanger, D. *Chem. Mater.* **2002**, *14*, 3946.

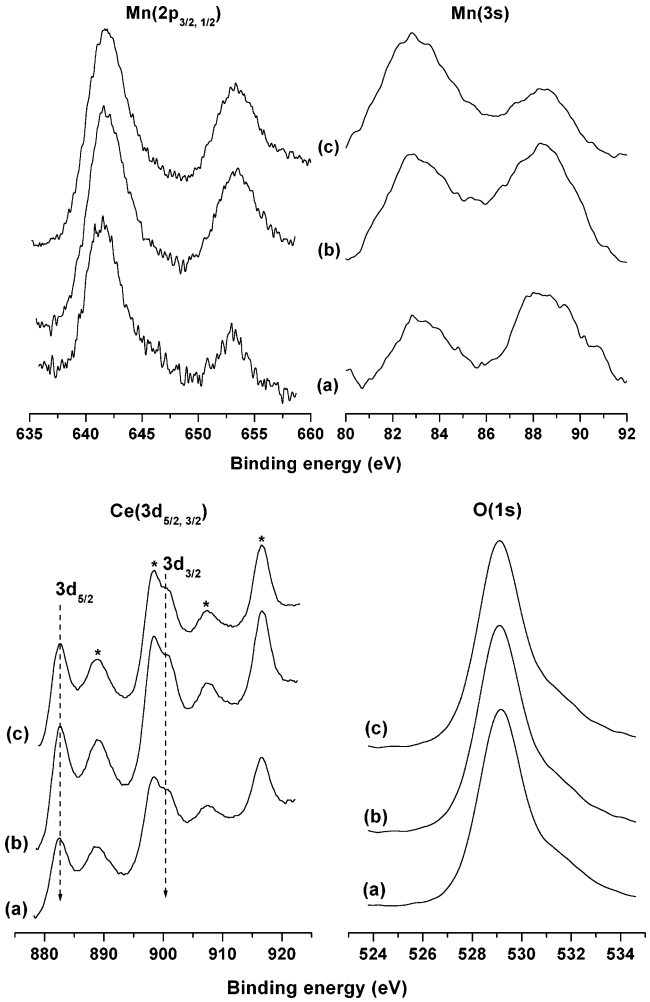

Figure 10. XPS spectra in the Mn(2p), Mn(3s), Ce(3d), and O(1s) core level regions for samples prepared by the combustion route. (a) $Ce_{0.99}Mn_{0.01}O_{2-\delta}$, (b) $Ce_{0.95}Mn_{0.05}O_{2-\delta}$, and (c) $Ce_{0.90}Mn_{0.10}O_{2-\delta}$.

Table 4. Mn(3s) Peak Splitting (ΔE) of Mn/CeO_2 Samples and Standard Oxides

sample	Mn(3s) peak splitting, ΔE (eV)	valence of Mn	phase	surface composition $(Mn/Ce)_{surf}$
$Ce_{0.99}Mn_{0.01}O_{2-\delta}$	5.5	2, 3		0.49
$Ce_{0.95}Mn_{0.05}O_{2-\delta}$	5.5	2, 3		1.53
$Ce_{0.95}Mn_{0.05}O_{2-\delta}$[a]	5.6	2, 3		2.85
$Ce_{0.90}Mn_{0.10}O_{2-\delta}$	5.6	2, 3		2.43
MnO_x	5.6	2, 3	MnO and Mn_3O_4	
MnO[b]	5.8	2	MnO	
Mn_3O_4[b]	5.5	2, 3	Mn_3O_4	
Mn_2O_3[b]	5.4	3	Mn_2O_3	
MnO_2[b]	4.8	4	MnO_2	

[a] Wet-impregnated sample. [b] Standard oxides of Mn from the literature.[41]

not show reflections corresponding to MnO_2 in the PXRD pattern (Figure 4).

The O(1s) spectra showed a main peak at 529.2 eV for all the Mn/CeO_2 samples, which is attributed to lattice oxygen (Figure 10). A small shoulder at 531.4 eV is attributed to oxygen in hydroxyl and carbonate impurities. The Ce(3d) peaks obtained from 1, 5, and 10 mol % Mn/CeO_2 samples are also shown in Figure 10. The spectra with satellite features (marked in the figure) correspond to CeO_2 with Ce in the +4 oxidation state.[44] The surface composition $(Mn/Ce)_{surf}$ calculated from the integrated peak area, the photoionization cross section, and the kinetic energy of the core levels[16] is found to be higher than that of the nominal bulk composition $(Mn/Ce)_{bulk}$ (Table 4). This indicates a homogeneous distribution and surface segregation of Mn ions on the CeO_2 surface.

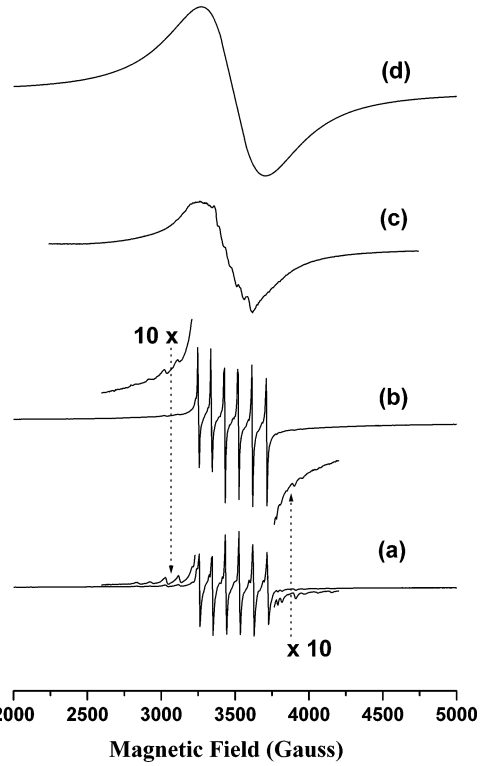

Figure 11. EPR spectra of the fresh samples prepared by the combustion route recorded at 298 K. (a) $Ce_{0.99}Mn_{0.01}O_{2-\delta}$; (b) $Ce_{0.95}Mn_{0.05}O_{2-\delta}$; (c) $Zr_{0.95}Mn_{0.05}O_{2-\delta}$, and (d) MnO_x.

The 5 mol % Mn/CeO_2 sample prepared by the wet-impregnation procedure showed a distinct $Mn(2p_{3/2})$ core level at 641.2 eV and a Mn(3s) ΔE of 5.6 eV. This value exactly matches with that of Mn_2O_3.[40] The Mn/Ce surface ratio of this sample is found to be higher than that of the sample prepared by the combustion route of same concentration (see Table 4). This suggests that all the Mn species in Mn/CeO_2 samples prepared by the wet-impregnation method are surface bound and do not form a part of the ceria lattice. This is in conformity with the PXRD data presented earlier (Table 1). However, the sample prepared by the combustion method showed a homogeneous distribution and surface segregation of Mn ions on the CeO_2 surface. The sample prepared by the coprecipitation method, in contrast, does not show any Mn core level features indicating a negligible concentration of Mn ions on the surface.

3.6. EPR Spectroscopy. There are at least three types of paramagnetic Mn^{2+} species in different Mn/CeO_2 samples prepared by the combustion method. These are isolated Mn^{2+} ions in defect sites with a noncubic symmetry (zero field splitting parameter $D \neq 0$, species A), isolated Mn^{2+} substituting for Ce^{4+} ions in the lattice having a cubic symmetry ($D = 0$, species B), and interacting Mn^{2+} ions located at the surface (species C). The 1 mol % Mn/CeO_2

(44) Sarma, D. D.; Hegde, M. S.; Rao, C. N. R. *J. Chem. Soc., Faraday Trans. II* **1981**, *77*, 1509.

sample showed an intense sextet line pattern and weak signals on either side of this pattern due to $|\pm^5/_2\rangle \leftrightarrow |\pm^3/_2\rangle$ and $|\pm^3/_2\rangle \leftrightarrow |\pm^1/_2\rangle$ electronic transitions (Figure 11). With increasing Mn content, the intensity of the sextet line pattern ($|-^1/_2\rangle \leftrightarrow |+^1/_2\rangle$ transition) increased but that of the outermost weak signals (due to $|\pm^5/_2\rangle \leftrightarrow |\pm^3/_2\rangle$ and $|\pm^3/_2\rangle \leftrightarrow |\pm^1/_2\rangle$ transitions) did not increase beyond ~2 mol %. This indicates that there are two types of isolated Mn^{2+} ions, one with a noncubic ($D = 215.3$ G) environment (species A) and the other with a cubic ($D = 0$) environment (species B). The concentration of the latter increases with the Mn content. The former-type isolated Mn^{2+} ions (species A) are attributed to those residing at the defect sites in the ceria lattice, and the cubic Mn^{2+} sites (species B) are those occupied in the substitutional sites. The g and hyperfine values ($g = 2.0023$ and $A_{Mn} = 93.6$ G) are consistent with the +2 oxidation state of Mn. Mn^{4+} ions show signals below the free spin g value (Mn^{4+} in MgO: $g = 1.994$ and $A = 76$ G at 290 K).[45] Hence, the EPR spectroscopy clearly reveals that Mn^{4+} ions are not present in the samples prepared by the urea combustion synthesis method. A similar conclusion is drawn also from the XPS and Rietveld refinement of the XRD pattern. At higher Mn concentrations (≥5 mol %), in addition to the above resolved spectral features a broad overlapping signal ($g \approx 2$) is also present. This corresponds to interacting Mn^{2+} species possibly located at the interstitial positions or at the surface (species C). An increasing concentration of the surface Mn ions (Mn/Ce ratio) with an increase of Mn content was also noted by XPS measurements. The concentration of substitutional Mn^{2+} sites increased by only 1.7 times (based on the EPR signal intensity) as against the expected 5 times increase in the 5 mol % compared to the 1 mol % Mn/CeO_2 sample. This indicates that the remaining part of the Mn ions form interacting Mn^{2+} species or may be present as Mn^{3+} species. The Mn^{3+} ions could be detected only at very low temperatures and high frequencies (e.g., W band). Reduction experiments, in fact, provided evidence for the presence of Mn^{3+} ions in Mn/CeO_2 samples. In those experiments, the Mn^{3+} was reduced to Mn^{2+} ions and the latter were detected by EPR spectroscopy.

Figure 11 also presents the effect of support on the type of Mn species formed. While the Mn/CeO_2 samples show resolved narrow signals corresponding to dispersed Mn species, Mn/ZrO_2 (prepared by a similar method using glycine as fuel) exhibits a broad spectral feature (Figure 11, curve c) corresponding to interacting Mn species. MnO_x prepared by the combustion method also shows a broad isotropic spectrum at $g = 2.005$ with a peak-to-peak separation of 434 G (Figure 11, curve d).

Evacuation of samples at elevated temperature has a marked effect on the spectral features. Multiple EPR plots of 1 mol % Mn/CeO_2 evacuated at different temperatures are shown in Figure 12. No major changes were observed until 523 K, and above that a significant decrease in the intensity of Mn^{2+} signals was noted. The hyperfine splitting constant reduced from 93.6 to 84.6 G. The signals due to $|\pm^5/_2\rangle \leftrightarrow |\pm^3/_2\rangle$ and $|\pm^3/_2\rangle \leftrightarrow |\pm^1/_2\rangle$ fine structure transitions

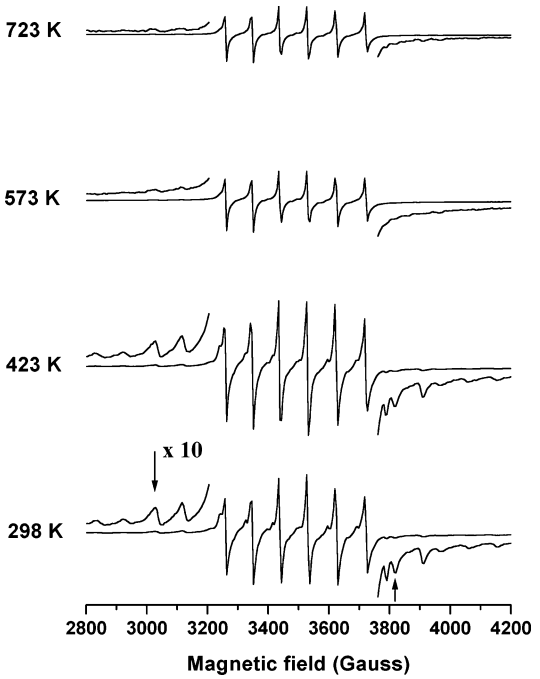

Figure 12. EPR spectra of the $Ce_{0.99}Mn_{0.01}O_{2-\delta}$ solid solution prepared by the combustion route thermo evacuated at different temperatures and recorded at 298 K.

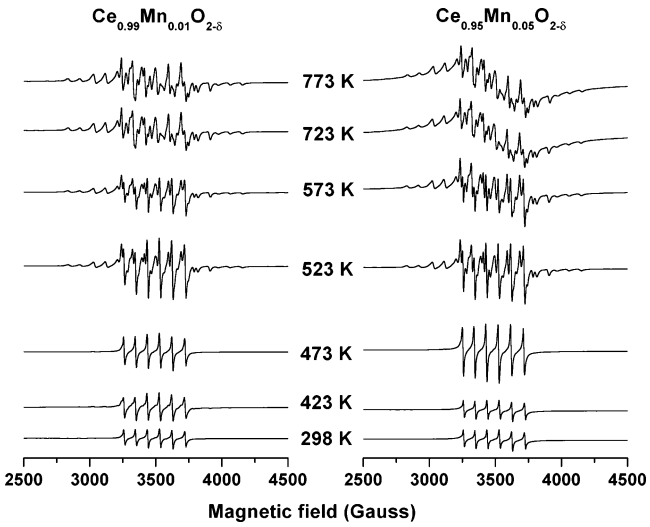

Figure 13. EPR spectra of $Ce_{0.99}Mn_{0.01}O_{2-\delta}$ and $Ce_{0.95}Mn_{0.05}O_{2-\delta}$ solid solutions prepared by the combustion route treated with hydrogen at different temperatures and recorded at 298 K.

(indicated by arrow; species A) disappeared. This may be explained on the basis of the earlier reports on Mn−APO-5 by Goldfarb et al. and Levi et al.[49−51] During high-temperature dehydration, the Mn^{2+} ions in the interstitial and surface locations migrate toward the Mn sites substituted in the ceria matrix and form weak interactions. As a consequence of spin−spin exchange interaction, the Mn^{2+} signals broaden beyond detection. Similar results are observed in the case of the 5 mol % Mn/CeO_2 sample.

The effect of hydrogen treatment on the Mn species in the 1 mol % Mn/CeO_2 samples is shown in Figure 13. The intensity of the EPR signals increased (by about 1.4 times) upon reacting with hydrogen at 473 K. The spectrum is very much like that for Mn^{2+} ions in a perfect cubic symmetry (species B). However, the EPR parameters are slightly

(45) Henderson, B.; Hall, T. P. P. *Proc. Phys. Soc.* **1967**, *90*, 511.

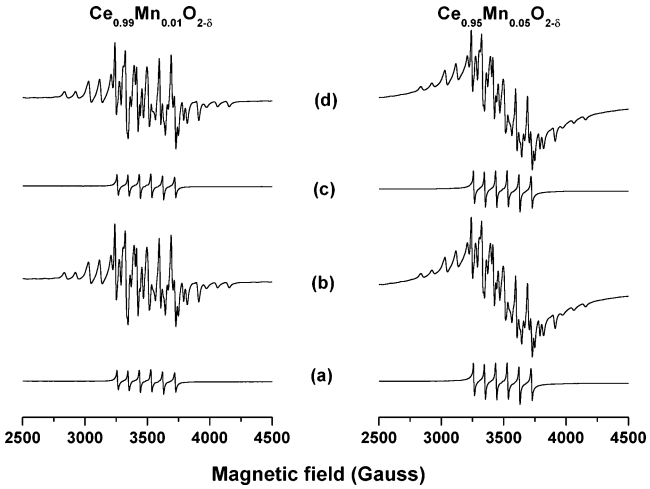

Figure 14. EPR spectra of the $Ce_{0.99}Mn_{0.01}O_{2-\delta}$ and $Ce_{0.95}Mn_{0.05}O_{2-\delta}$ solid solutions prepared by the combustion route showing the reversible redox behavior of the Mn species in ceria. (a) Fresh sample evacuated at 773 K; (b) reduced at 773 K; (c) reoxidized at 573 K; and (d) rereduced at 773 K. The sample is reduced at 773 K in the flow of hydrogen, and oxidation is done at 573 K in the flow of air and recorded at 298 K.

different ($g = 2.0045$ and $A = 92.6$ G) from those observed for the untreated samples ($g = 2.0023$, $A_{Mn} = 93.6$ G). The increase in the signal intensity is confined to only the central six-line hyperfine pattern and not to the signals due to species A. This suggests that some Mn^{3+} species are also present in the lattice substitutional locations, which get reduced to Mn^{2+} upon reaction with molecular hydrogen.

At still higher reduction temperatures (523 K), additional Mn^{2+} signals corresponding to Mn ions in a very low-symmetry octahedral environment were observed ($g = 2.0024$, $A = 83.6$ G, and $D = 424.2$ G; see Figure 13). This suggests that there exists some Mn^{3+} possibly on the surface that gets reduced upon reaction with hydrogen at 523 K resulting in these types of species. The signal due to high-symmetry Mn species (species B) overlaps with these additional signals. As the temperature is increased to 573 K, more and more surface Mn^{3+} species get reduced. At high temperatures (above 723 K) a broad background signal also appeared due to the formation of a higher amount of paramagnetic Mn species. This is more evident in the case of the 5 mol % Mn/CeO_2 sample (Figure 13). At 723 K, an amount of Ce^{4+} ions got reduced to Ce^{3+} and showed a weak, overlapping signal at $g = 1.965$. At 773 K, weak, additional multiplet hyperfine patterns ($A_{Mn} = 42.5$ G) were observed in the low field region at $g = 3$. These features are attributed to formation of $-Mn^{2+}-O-Mn^{2+}-$ dimeric species. At higher temperatures the reduced Mn^{2+} ions migrate forming dimers and interacting clusters of smallest size.

To confirm the reversible redox behavior, the samples, which were reduced in hydrogen (773 K), were reoxidized with air at 573 K (Figure 14). The reduced samples showed a multiplet spectrum, corresponding to ions in both high- and very low-symmetry octahedral environments, whereas the oxidized samples showed mainly a cubic-type Mn spectra. The Mn^{3+} ions could be reduced and reoxidized in several cycles. The facile redox behavior of the Mn^{3+} species is an interesting property that could be exploited in many oxidation−reduction reactions catalyzed by these Mn/CeO_2 samples.

The EPR spectra of Mn/CeO_2 samples prepared by different methods are significantly different as shown in Figure 15. While the samples prepared by the wet-impregnation method showed a broad signal attributable to clustered Mn ions,[46,47] those prepared by coprecipitation showed a broad feature overlapped with six hyperfine features corresponding to the presence of both interacting and distorted Mn^{2+} ions. The samples prepared by the solution combustion method, on the other hand, showed a well-resolved six line pattern mainly due to highly dispersed Mn^{2+} ions; these

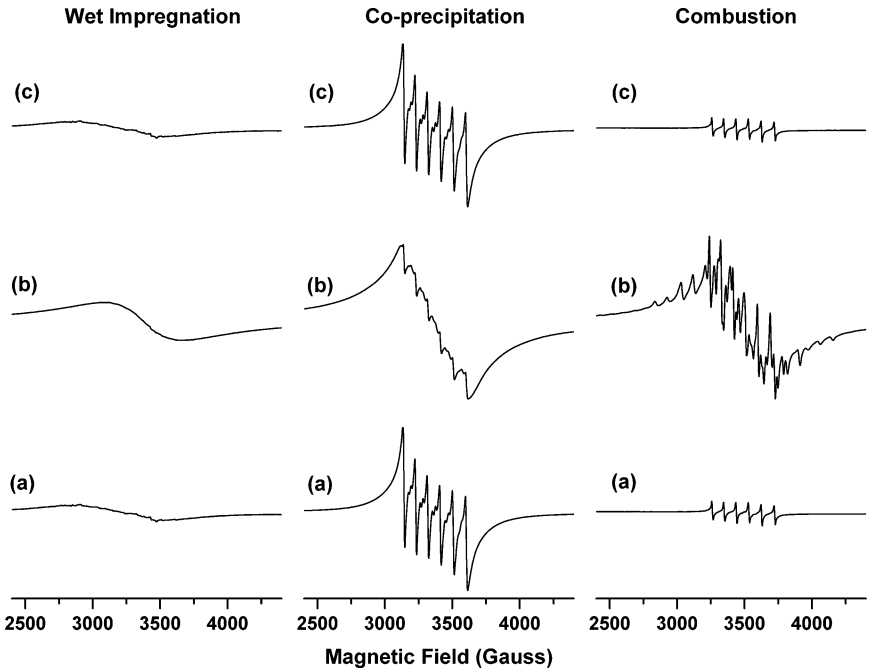

Figure 15. EPR spectra of the $Ce_{0.95}Mn_{0.05}O_{2-\delta}$ solid solutions prepared by various methods showing the reversible redox behavior of the Mn species in ceria. (a) Fresh sample evacuated at 773 K; (b) reduced at 773 K and reoxidized at 573 K. The sample is reduced at 773 K in the flow of hydrogen, and oxidation is done at 573 K in the flow of air and recorded at 298 K.

samples do not contain clustered Mn species unlike in the wet-impregnated sample. The relatively weak intensity of EPR signals for the samples by the solution combustion method (see Figure 15) suggests, in agreement with the UV−visible spectroscopy results (Table 2), that Mn is present mainly in the +3 oxidation state in these samples.

The Mn^{3+} species could be reversibly reduced and reoxidized. The sample prepared by wet-impregnation upon reduction with hydrogen, at 773 K, showed a broad signal corresponding to clustered Mn^{3+} species. The reduced sample prepared by the coprecipitation method showed a broad feature with overlapping ^{55}Mn hyperfine features. The sample by solution combustion synthesis, on the other hand, showed a spectrum enriched with well-resolved fine structure and hyperfine features, of a highly dispersed Mn species. The comparative study, thereby, clearly indicates that the method of sample preparation influences the Mn speciation and its oxidation state. Samples by the wet-impregnation method contained clustered MnO_x surface species, and those by the coprecipitation method contained isolated Mn species along with the clustered species. Interestingly, the samples prepared by the solution combustion method using urea as fuel contain highly dispersed Mn species in ceria. Earlier reports showed that the solid-state synthesis method yields only the clustered Mn species.[48] Qi et al. in their findings showed that samples prepared by using the citric acid method gave a high NO conversion, irrespective of the surface area.[17] This enhancement in activity was attributed to dispersed Mn species. On the basis of our spectral results, it appears that a Mn dispersion of much higher order is possible in the samples prepared by solution combustion synthesis than in samples prepared by other known methods.

4. Summary and Conclusions

The following conclusions can be drawn from the structural and spectroscopic characterization studies of MnO_x−CeO_2 samples prepared by the solution combustion route:

(a) In Mn/CeO_2 samples prepared by the solution combustion synthesis method, the Mn ions are present mainly in +2 and +3 oxidation states. The XRD, XPS, TPR, and EPR investigations provide no evidence for the presence of manganese species in the +4 oxidation state (MnO_2).

(b) A progressive decrease in the unit cell parameter with Mn concentration in ceria and the absence of a separate manganese oxide-like phase (large crystallites) reveal the formation of homogeneous $Ce_{1-x}Mn_xO_{2-\delta}$ solid solutions in the concentration range of $x = 0.01-0.20$. $(Mn/Ce)_{surf}$ values also support the uniform distribution of Mn in these samples.

(c) Sintering of ceria is attenuated by incorporation of Mn ions through the combustion procedure. The study reveals that the Mn ions occupying the ceria lattice defect sites are responsible for controlling the sintering process.

(d) DRUV−vis and EPR spectral observations of the samples reveal that the predominating Mn species are in the +3 oxidation state and that Mn dispersion and the −Mn−O−Ce− interactions are high in these samples.

(e) EPR spectroscopic studies also point out the presence of three different types of Mn species with respect to their local environment and coordination.

(f) Reduction followed by reoxidation experiments with dry hydrogen and air, respectively, at elevated temperatures revealed that the Mn^{3+} species in the CeO_2 matrix exhibit facile redox behavior.

(g) The reducibility of the manganese species is enhanced when it is present in the ceria lattice. The temperature maximum for the reduction process (T_{max}) for Mn occurs at a lower temperature in Mn/CeO_2 compared to MnO_x, due to a synergistic effect between the Mn^{n+} and Ce^{4+} ions in these samples.

The method of preparation (wet-impregnation, coprecipitation, solid-state synthesis, and citric acid and solution combustion syntheses) influences the type of Mn species (dispersed versus interacting manganese ions) formed and their oxidation state. Samples prepared by the wet-impregnation method contained clustered MnO_x surface species with little interaction with ceria. Those prepared by the coprecipitation method contained isolated Mn species, including Mn^{4+} oxide along with other clustered Mn oxides. These samples sinter substantially on thermal treatment. The solution combustion method provides a way to prepare Mn/CeO_2 samples enriched with reducible Mn^{3+} species along with Mn^{2+} species in the ceria matrix. These are significantly different from the samples prepared by other techniques.

Acknowledgment. B.M. thanks CSIR, New Delhi, for a research fellowship. The authors are thankful to Dr. S. P. Mirajkar for his help with the TPR experiments.

CM050401J

(46) Abi-Aad, E.; Bennani, A.; Bonnelle, J. P. *J. Chem. Soc., Faraday Trans.* **1995**, *91*, 99.
(47) Figaj, M.; Becker, K. D. *Solid State Ionics* **2001**, *141*, 512.
(48) de Biasi, R. S.; Grillo, M. L. N. *J. Phys. Chem. Solids* **2003**, *64*, 1365.
(49) Goldfarb, D. *Zeolites* **1989**, *9*, 509.
(50) Wu, J. Y.; Chien, S. H.; Wan, B. Z. *Ind. Eng. Chem. Res.* **2001**, *40*, 94.
(51) Levi, Z.; Raitsimring, A. M.; Goldfarb, D. *J. Phys. Chem.* **1991**, *95*, 7830.
(52) Bentrup, U.; Bruckner, A.; Richter, M.; Fricke, R. *Appl. Catal. B* **2001**, *32*, 229. Reddy, B. M.; Khan, A.; Yamada, Y.; Kobayashi, T.; Loridant, S.; Volta, J. C. *J. Phys. Chem. B* **2002**, *106*, 10964.
(53) Vincente, M. A.; Belver, C.; Trujillano, R.; Rives, V.; Alvarez, A. C.; Lambert, J.-F.; Korili, S. A.; Gandia, L. M.; Gil, A. *Appl. Catal. A* **2004**, *267*, 47.
(54) Kapteijn, F.; Langeveld, A. D. V.; Moulijn, J. A.; Andreini, A.; Vuurman, M. A.; Turek, A. M.; Jehng, J.-M.; Wachs, I. E. *J. Catal.* **1994**, *150*, 94.